Clays and Clay Minerals, Vol. 54, No. 3, 390–401, 2006.

X-RAY DIFFRACTION LINE BROADENING ON VIBRATING DRY-MILLED TWO CROWS SEPIOLITE

JOAQUIN BASTIDA[1], MAREK A. KOJDECKI[2], PABLO PARDO[1] AND PEDRO AMORÓS[3]

[1] Departamento de Geología, Universidad de Valencia, 46100 Burjasot, Valencia, Spain
[2] Instytut Matematyki i Kryptologii, Wojskowa Akademia Techniczna, 00-908 Warszawa, Poland
[3] Instituto de Ciencia de Materiales, Universidad de Valencia, 46071 Paterna, Valencia, Spain

Abstract—A reference sample of sepiolite and products of its comminution by vibrating dry-milling have been studied using X-ray diffraction (XRD) line-broadening analysis, complementary field emission scanning electron microscopy (FESEM) images and surface area measurements. The apparent crystallite sizes determined *via* XRD are in agreement with observations on FESEM images. The sepiolite aggregates consist of lath-shaped agglutinations of prisms and pinacoids elongated along [001], each lath including several crystallites in that direction. The surface area magnitudes are in the range of previous experimental measurements of other sepiolites. The results obtained show the effectiveness of vibro-milling as the procedure to use for the comminution of sepiolite.

Key Words—Crystallite Size, Crystalline Lattice Strain, Line Broadening, Nevada Sepiolite, Reference Clay, Sepiolite, Surface Area, X-ray Diffraction.

INTRODUCTION

Two Crows sepiolite is a rather pure sepiolite mineral (Post, 1978) considered as a useful standard in comparing sepiolites from different sources (Post and Janke, 1984). Specimens of this mineral were made available through the Source Clays Repository of The Clay Minerals Society.

Sepiolite is an important industrial mineral found in Spain, which is the largest producer in the world (Virta, 2004; Wilson, 2004); small quantities are also mined in Turkey and in the USA (Santarén and Alvarez, 1994; Harben and Kuzwart, 1999). The main petrographical features and geological occurrences were listed by Caillère *et al.* (1982), Alvarez (1984) and Jones and Galán (1988). Two main types of geological occurrences can be found: sedimentary and hydrothermal (Alvarez, 1984; Lopez Galindo and Sanchez Navas, 1989).

Reviews of the sepiolite structure were given by Bailey (1980) and Caillère *et al.* (1982). The structure model of Brauner and Preisinger (1956) with the compositional formula for the half unit-cell of:

$$(Mg_{8-y-z}R^{3+}_y)(Si_{12-x}R^{3+}_x)O_{30}(OH)_4(OH_2)_4R^{2+}_{(x-y+2z)/2}8H_2O$$

was confirmed by the results of an electron diffraction structure study by Rautureau (1974), Rautureau and Tchoubar (1974, 1976) and Yücel *et al.* (1980, 1981).

Sepiolite appears frequently as laths clumped together to form frayed bundles on a macroscopic scale (Harben and Kuzwart, 1999). The typical dimensions of microscopic sepiolites are: 2000–20,000 Å long × 100–3000 Å wide × 50–100 Å thick, according to Martin Vivaldi and Robertson (1971); greater values (150–1000 Å thick, on prevalent (110) faces) were found in macroscopic fibers (cm long) of the samples studied by Rautureau and Tchoubar (1976).

The study by Yücel *et al.* (1980) includes high-resolution electron micrographs and reports fibrous crystallites with average lengths of ~500 Å and small development in cross-section.

The micromorphological analyses of fibrous particles are frequently reported in research on carcinogenic hazards, and the greatest correlation coefficients with carcinogenic hazard were found for fibers >8 μm long with diameters of <0.25 μm (Stanton *et al.*, 1981); that range of length is unusual in sedimentary sepiolites. The sepiolite case was considered by Santarén and Alvarez (1994) in the assessment of the health effects of mineral dusts, and the results of different studies performed for sedimentary sepiolites (epidemiological studies, animal experiments and '*in vitro*' tests) have been consistently negative, showing a low intrinsic biological activity and an absence of diseases that could be exposure-related.

There is a wide range of applications for sepiolite based mainly on sorptive, rheological and catalytic properties, extensively reported by Alvarez (1984).

Relevant microstructural properties such as surface area and porosity were reviewed by Serratosa (1979) and Alvarez (1984). The low effectiveness of ball-milling comminution for increasing surface area in sepiolite has been found by Cornejo and Hermosin (1988).

Microstructural analysis for powder XRD line broadening, producing results concerning crystallite size and lattice strain, is a conventional technique in materials science (see Guinebretière, 2002); the recent improvements in XRD instruments, data collection and data

* E-mail address of corresponding author:
bastida@uv.es
DOI: 10.1346/CCMN.2006.0540310

Copyright © 2006, The Clay Minerals Society

https://doi.org/10.1346/CCMN.2006.0540310 Published online by Cambridge University Press

treatment allow the applications of XRD line-broadening analyses to a wide range of polycrystals as shown, for example, in the review by Langford and Louër (1996) or in works by Snyder *et al*. (1999) and Mittemeijer and Scardi (2003). A review of XRD microstructural analyses of sheet silicates can be found in Clausell (2001). As all these procedures lead to the calculation of apparent crystallite sizes (Wilson, 1967), different techniques, mainly high-resolution electron microscopy, are used to compare and better explain the results.

References to sepiolite 'crystallinity' can be found in some studies of sepiolites (Lopez Galindo and Sanchez Navas, 1989; Vicente *et al*., 1994). The literature on sepiolite processing includes much information about evolution of microstructural characteristics involved in sepiolite processing (micromorphology, particle size and particle distribution, porosity, surface area,...) but there are no XRD microstructural data (crystallite size and/or microstrains) concerning sepiolites (except for the study of ball milling by Cornejo and Hermosin, 1988), so it is useful to show results for the evolution of these characteristics in a pure reference sample of sepiolite.

The evolution of the real XRD microstructure (including the evolution of crystallite shape) of this sepiolite has been performed recently (Kojdecki *et al*., 2005) using deconvoluted pure line profiles, influenced only by the crystalline microstructure, obtained by using a stable algorithm (Kojdecki, 2001) and a very good agreement between an XRD-calculated surface area and that calculated from nitrogen adsorption has been found during the increase in surface area.

The aim of the present work is to show the evolution of the XRD line broadening of sepiolite on a milling process (vibrating-cup milling) using a simplified method. The Voigt function method was performed and these results are compared with those obtained by other techniques (the XRD Warrren-Averbach method, surface area, and FESEM measurements).

MATERIALS

The material studied is the reference sample Sep-Nev-1 provided by the Source Clays Repository of The Clay Minerals Society, Purdue University, 915 West State Street, West Lafayette, IN 47907-2054, USA. Information about the occurrence, origin, physical characteristics, as well as XRD powder data (with Miller indices taken from Grim, 1968, and Borg and Smith, 1969), an infrared spectrum, the thermal characteristics, chemical analysis results and scanning electron micrographs can be found in Post (1978).

The chemical composition (%) is: SiO_2 54.0, Al_2O_3 0.5, TiO_2 <.001, Fe_2O_3 0.81, FeO <0.1, MnO 0.11, MgO 23.3, CaO 1.25, Na_2O 2.1, K_2O 0.15, P_2O_5 0.02, LOI 19.2. The structural formula is: $(Ca_{0.2}Na_{0.6}K_{0.03})[Mg_{5.81}Al_{0.09}Mn_{0.01}Fe^{III}_{0.09}][Si_{8.00}]O_{20}(OH)_4$; octahedral charge: +0.18, tetrahedral charge: 0.0, interlayer charge: +0.18, unbalanced charge: +1.03; extra Si: 0.02; Mg deficiency: 0.65.

METHODS

Sample preparation

An experimental mechanical comminution was performed using a laboratory vibrating cup mill (Fritsch Pulverisette 9), with agate grinding sets (1 disk + 1 ring) working at 1500 rpm.

Granules of <2 mm of the reference sample were obtained by knife cutting, and 15 g samples of this material, free of visible impurities, were treated by dry grinding for different periods using the vibrating mill above. The selected grinding times were 3, 6, 12, 24, 36, 48 and 60 s, the samples obtained are labeled N3, N6, N12, N24, N36, N48 and N60, respectively.

X-ray diffraction

The equipment used was a Philips XPERT diffractometer (PW3020, with Cu anode, and graphite monochromator), working at 40 kV, 50 mA, with the sample holder spinning. The primary optics were: without beta filter, with 0.04 rad Soller slits, 1º divergence slit, 15 mm beam mask. The secondary optics were: without collimator and beta filter; with 1º anti-scatter slit; 0.10 mm receiving slit and 0.04 rad Soller slit.

Data collection was performed by step scanning, using a 0.02º2θ step-size with 1 s counting time for general identification and the same step-size and variable counting time (according to the peak intensity), for the different peaks selected for microstructural analysis (these were 4 s for the 110 peak and 16 s for the other selected peaks). The powder was placed in the sampler by backpressing to provide an unoriented powder sample (Niskanen, 1964).

The EVA program of the Diffrac-Plus package (Bruker AX Systems) was used to manage the data files after conversion of the format. Sepiolite was identified using the Search program (based on Causin *et al.*, 1989) of this package, working on the PDF-2 database (ICDD, 2002), by applying the general procedure for identification of sheet silicates of Warshaw and Roy (1961), performed with unoriented powder and oriented aggregates.

Morphological approach

A morphological approach is needed to select peaks for XRD microstructural analysis as well as to compare the obtained results with micromorphological observations by electron microscopy. The forms of greater morphological importance can be found in a first approach by considering lattice parameters and space group (according to the law of Donnay and Harker, 1937). It has been performed for sepiolite using the crystallographic data of Brauner and Preisinger (1956) with the program Shape (Shape v.7.0, of Shape

https://doi.org/10.1346/CCMN.2006.0540310 Published online by Cambridge University Press

Table 1. Central distances for different forms (from the *Shape* program).

Figure	Central distances (D_{hkl}, c.d.u.)									k value in the formula used for D_{hkl} =		
	hkl	010	110	130	100	011	150	111	120	$k(1/d_{hkl})$	$\exp(-kd_{hkl})$	$d_{hkl}\exp(-kd_{hkl})$
A		1	1.12	1.8	2	2.59	2.69	2.78	2.83	0.6		
B		1	1.16	1.82	1.97	2.29	2.33	2.37	2.39		0.15	
C		1	2.15	20.4	28.8	55.5	59.8	63.8	66			0.6
D		1	4.3	407	870	3965	4783	5624	6132	1		
E		1	2.4	36.8	58	144	161	177	187		0.6	

hkl = Miller index of the considered face; D_{hkl} = central distance for the (*hkl*) face in arbitrary units (c.d.u.); d_{hkl} = interplanar spacing (Å) between *hkl* planes; A, B, C, D and E = figures corresponding to combinations of the indicated forms with different central distances (A and C are shown in Figure 1). The form {*hkl*} has morphological expression if the central distance is small enough.

Software) of Dowty (1980). A form {*hkl*} has morphological expression if the value of the central distance D_{hkl} (related to the d_{hkl} spacing and with the growth rate of the face (*hkl*)) is small enough. Table 1 shows the values of central distances for different faces considering different possible relationships between central distances and d_{hkl} values. Figure 1 shows the appearance of the combinations produced of forms A and C of that Table. It must be noted that the most probable forms are parallel to (001) and that a (100) face with small central distances is not achieved; the limiting faces of prisms and pinacoids parallel to 001 show limited development, with the prevalent forms {110} and {010}. The very limited morpholgical expression of the {131} and {111} forms (of faces not parallel to [001]), is easily visible.

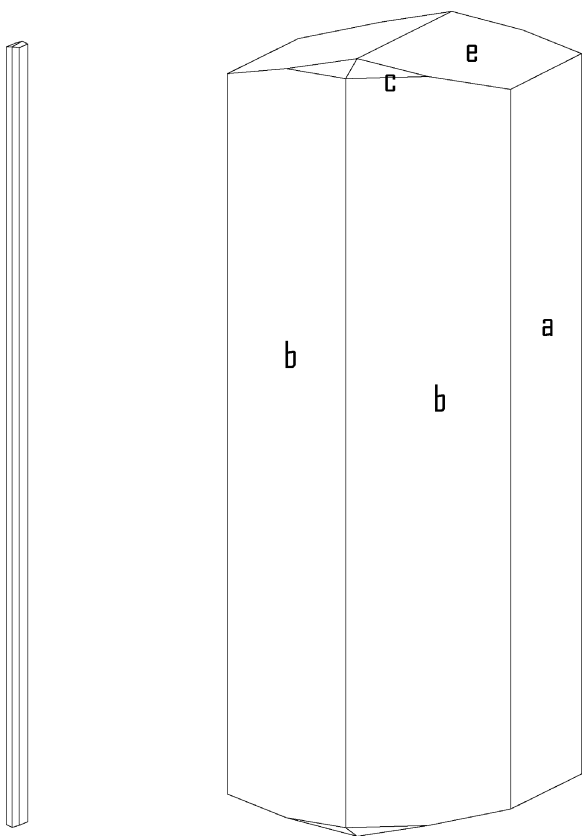


Figure 1. Combinations of forms A (right) and C (left) of Table 1: *a* = {010}, *b* = {110}, *c* = {111}, *e* = {011}.

Microstructural evaluation of X-ray diffraction data

Peaks of relatively high intensity, uniquely indexed, not excessively overlapped (to avoid difficulties with profile fitting) and corresponding to planes of greater morphological importance (and so allowing the interpretation of the results obtained by comparison with their morphological appearance in micrographs), were selected for the XRD microstructural analysis.

The microstructural analyses for the 010 and 110 directions of diffraction will produce relevant results to compare with morphology as shown above. The selection of peaks for microstructural analysis will be performed by considering the method to be used (single-line or multiple-line analysis), the intensities (greater counting rates will be needed for peaks of lesser intensity) and the overlapping of indexed peaks (limited enough to allow the fitting of profiles to the XRD powder pattern).

Background subtraction was performed using the enhanced method of the EVA program in the range shown in Figure 2 (upper) for the different samples, and then the peaks were fitted to split Voigt functions using the Profile program of the package Diffrac-AT (Socabim-Bruker) that provides the properties of the $K\alpha_1$ profiles from the collected raw data. Instrumental profiles were obtained from the experimental XRD pattern of the LaB_6 powder (NIST SRM640a standard reference material). The reliabilities (R_{wp} values) for the modeled profiles were always <2.5 and not far from the theoretical reliabilities of the experimental peaks for samples ground for up to 24 s. The same is true for larger grinding times except for the 130 and 260 reflections showing greater R_{wp} values (see Table 2). The poor reliabilities in the fitting of 260 could be related to the large overlap with the 151 reflection. The good reliabilities for the 110 reflection may be related to the extremely low relative intensity of the 020 reflection (if present).

https://doi.org/10.1346/CCMN.2006.0540310 Published online by Cambridge University Press

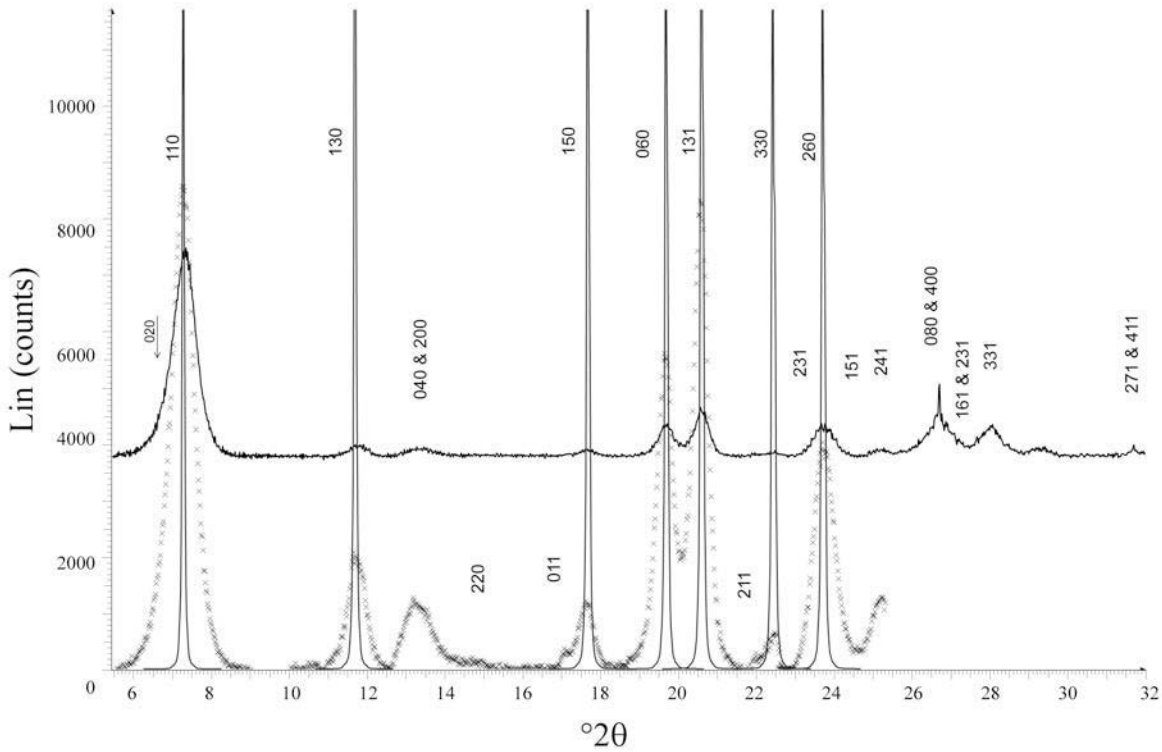


Figure 2. Upper: XRD pattern of sample N3 used for identification (some Miller index labels are included for overlapping peaks indicated in the text). Lower: experimental peaks used for microstructural analysis of sample N3 (fitted profiles of the studied lines are included as well as the narrow instrumental profiles).

The Warren-Averbach analysis (Bertaut, 1950; Warren and Averbach, 1950; Warren, 1955) using the Wincrysize program (of Bruker AXS) was performed for apparent crystallite size calculation by double-line analyses of reflections 110−330 and 130−260 (results shown in Table 3).

The simplified method of the Voigt function (Langford, 1978, 1992), relying on modeling the peaks by split Voigt functions (Delhez *et al*., 1982; de Keijser *et al*., 1982, 1983) has also been used for the above reflections as well as for those at 150 and 131 (results shown in Table 2). This is a very useful simplified method (see a ranking of quality of methods in Vermeulen and Delhez, 2004) allowing the separation of the line broadening related to crystallite size and that related to other sources; the method provides a value of volume-weighted average apparent crystallite size $<D_v>$ and another one, *e*, as a representative of lattice strain (the existence of microstrains can be expected as a consequence of energetic procedures such as grinding and the contribution from strain has also been identified in this work by the Warren-Averbach method for the 110 and 130 reflections). Different values are found for volume-weighted $<D_v>$ values and area-weighted average column lengths, *L*, of the Warren-Averbach method (providing smaller values as shown by Langford, 1992) and good correlation between both values was found in several works (*e.g.* Serrano *et al*., 1996; Clausell, 2001, for mullites and kaolinites, respectively).

Electron microscopy

An Hitachi 4100 field emission scanning electron microscope operating at 35 kV accelerating voltage was used. The image collection was carried out using the program EMIP (supplied by Hitachi). The samples of sepiolite were prepared by setting a drop of a diluted water suspension of powder on a metallic strip. After drying the water drop, the metallic strip was pasted to a FESEM holder and was coated with gold-palladium using a Struers Epovac device and then the measurements were performed directly by analyzing the images using the program Leica Q500MC QWIN v01.

Surface area

Nitrogen adsorption isotherms were measured using a Micromeritics ASAP 2010 instrument for the samples, degassed over 15 h at 150ºC and 10^{-6} Torr prior to measurement, and the surface area was determined by using the BET method (Brunauer *et al*., 1938).

RESULTS AND COMMENTS

The sample ground for 3 s was used to verify the mineralogical composition. Only sepiolite was identi-

https://doi.org/10.1346/CCMN.2006.0540310 Published online by Cambridge University Press

Table 2. X-ray data and microstructural parameters (obtained by the Voigt function method) for the peaks studied in the different samples.

hkl	Sample	TR	R_{wp}	2θ	N	H	FWHM	β	ϕ	$<D_v>$	*e*
110	STD	1.39	0.88	7.356	464	6274	0.052	0.07396	0.70312		
	N3	1.41	1.58	7.250	5971	5887	0.720	1.01427	0.70987	120	0.02814
	N6	1.41	1.58	7.314	5848	5424	0.743	1.07817	0.68913	104	0.02468
	N12	1.57	1.82	7.290	4343	4048	0.740	1.07288	0.68974	104	0.02480
	N24	1.79	1.66	7.294	3563	2884	0.872	1.23544	0.70582	96	0.03303
	N36	1.91	1.96	7.260	2804	2063	0.964	1.35919	0.70925	88	0.03752
	N48	2.04	2.03	7.313	2557	1616	1.065	1.58230	0.67307	65	0.02982
	N60	2.59	2.71	7.378	1053	450	1.519	2.34000	0.64915	40	0.02495
130	STD	1.17	0.91	11.867	737	9734	0.052	0.07571	0.68680		
	N3	1.97	2.44	11.685	832	1336	0.539	0.62275	0.86551	833	0.02159
	N6	2.05	2.23	11.800	704	1080	0.536	0.65185	0.82227	417	0.01939
	N12	2.15	2.38	11.780	644	871	0.618	0.73938	0.83584	412	0.02311
	N24	1.92	2.84	11.872	673	907	0.625	0.74201	0.84231	444	0.02351
	N36	4.50	15.10	11.681	475	608	0.646	0.78125	0.82688	347	0.02387
	N48	5.95	21.40	11.766	329	326	0.699	1.00920	0.69263	114	0.01485
150	STD	1.03	1.43	17.766	1083	13790	0.056	0.07854	0.71306		
	N3	1.17	2.08	17.624	412	784	0.449	0.52551	0.85441	857	0.01159
	N6	2.25	2.11	17.690	276	528	0.403	0.52273	0.77096	357	0.00837
	N12	2.39	2.27	17.679	295	547	0.409	0.53931	0.75838	317	0.00814
	N24	2.42	2.41	17.697	226	358	0.497	0.63128	0.78728	318	0.01087
	N36	2.10	2.18	17.676	178	257	0.548	0.69261	0.79121	292	0.01215
060	STD	1.00	1.40	19.506	1189	14973	0.057	0.07941	0.71780		
	N3	1.46	1.39	19.662	2258	3583	0.463	0.63020	0.73469	232	0.00751
	N6	1.48	1.81	19.707	1993	2714	0.508	0.73434	0.69178	161	0.00632
	N12	1.49	1.91	19.674	1963	2628	0.521	0.74696	0.69750	162	0.00680
	N24	1.61	1.69	19.664	1473	1846	0.549	0.79794	0.68802	145	0.00662
	N36	1.50	1.87	19.630	1391	1739	0.547	0.79988	0.68385	142	0.00635
	N48	1.55	1.68	19.630	1727	1700	0.740	1.01588	0.72843	132	0.01172
	N60	1.76	1.89	19.576	627	593	0.774	1.05734	0.73203	128	0.01251
131	STD	0.98	1.35	20.586	1257	15734	0.057	0.07989	0.71347		
	N3	1.48	1.42	20.559	3411	5570	0.445	0.61239	0.72666	231	0.00664
	N6	1.49	1.91	20.620	2544	3882	0.476	0.65533	0.72635	214	0.00707
	N12	1.47	1.82	20.593	3235	4547	0.489	0.71146	0.68732	168	0.00371
	N24	2.39	2.27	20.603	2516	3369	0.525	0.74681	0.70299	166	0.00681
	N36	1.50	1.53	20.560	2039	2853	0.560	0.71469	0.78356	144	0.01041
	N48	1.53	1.53	20.560	2675	3094	0.611	0.86458	0.70670	124	0.00966
	N60	1.17	2.08	20.657	1017	774	1.001	1.31395	0.76182	118	0.01729
330	STD	1.00	1.40	22.500	1369	17950	0.057	0.07989	0.71347		
	N3	1.94	1.86	22.518	470	967	0.336	0.48604	0.69130	260	0.00359
	N6	1.98	1.87	22.476	568	948	0.415	0.59947	0.69228	205	0.00451
	N12	1.87	1.75	22.600	396	643	0.426	0.61625	0.69128	197	0.00457
	N24	1.70	1.53	22.500	295	478	0.427	0.61767	0.69131	197	0.00460
	N36	1.59	0.25	22.432	140	286	0.338	0.48917	0.69097	257	0.00362
260	STD	0.98	1.35	23.600	1434	17950	0.057	0.07989	0.71347		
	N3	1.78	4.20	23.700	1045	1155	0.626	0.90443	0.69215	130	0.00648
	N6	1.78	4.26	23.706	1047	1178	0.615	0.88912	0.69170	132	0.00634
	N12	1.87	3.34	23.791	895	929	0.667	0.96331	0.69240	121	0.00690
	N24	1.89	2.91	23.677	714	717	0.689	0.99607	0.69172	117	0.00713
	N36	1.91	2.26	23.670	527	495	0.737	1.06456	0.69230	109	0.00767
	N48	1.91	1.85	23.643	409	370	0.764	1.10459	0.69166	104	0.00792

TR = Theoretical reliability = $100[\Sigma I_{obs}/\Sigma I_{obs}^2]^{1/2}$; R_{wp} = reliability of profile fitting = $100[w(I_{obs}-I_{calc})^2/\Sigma w I_{obs}^2]$ where $w = 1/[\sigma(I_{obs}^2)]$; θ = Bragg angle (°). *N* = normalized peak area; *H* = height of the peak (cps); FWHM = full width at half maximum (°); β = integral breadth (°); ϕ = shape parameter; $<D_v>$ = mean volume-weighted apparent crystallite size (Å); *e* = strain parameter.

https://doi.org/10.1346/CCMN.2006.0540310 Published online by Cambridge University Press

Table 3. Crystallite sizes obtained by the Warren Averbach method.

Sample	Dif Av L (%)	Av $L_{[110]}$	Mrf $L_{[110]}$	Dif Mrf L (%)	SMRF
N3	–	86	66	–	–
N6	0.09	94	77	0.14	0.0054
N12	−0.49	63	43	−0.79	0.0000
N24	0.10	70	70	0.39	0.0000
	Dif Av L (%)	Av $L_{[130]}$	Mrf $L_{[130]}$	Dif Mrf L (%)	
N3	–	68	30	–	0.0046
N6	0.17	82	36	0.17	0.0079
N12	−0.28	64	29	−0.24	0.0051
N24	−0.42	45	25	−0.16	0.0000
N36	0.04	47	24	−0.04	0.0000
N48	−0.09	43	23	−0.04	0.0000

Av L = average column length (for the indicated direction, Å); Mrf L = position (column length) of maximum of relative frequency of column length (for the indicated direction, Å); Dif = difference from the previous sample; – = no result; SMRF = strain at column length of maximum relative frequency.

fied; the best match was found for the calculated ICDD file 75-1597 (107 matching lines, 2 non-matching lines, FOM = 0.15), and the second score (32 lines, 0 non-matching, FOM = 0.78) for the experimental 26-1226 file (corresponding to Nagata *et al*., 1979).

Figure 2 (upper) shows part of the powder XRD pattern used for identification. According to the micro-morphological approach used, the most relevant lines, selected for microstructural analysis, are *hh*0 and 0*k*0. Additional reflections of relatively high intensity, of unique indexation and without severe overlapping, were also considered, and the selected set was: 110, 130, 150, 060, 131, 330 and 260. The complexity of the pattern must be noted, having a great number of peaks but mainly of low intensity (there are no values >1% at spacings <2.389 Å and most of the peaks are <1% of the intensity of the strongest peak). The selected peaks were registered at a greater counting rate. The peaks analyzed

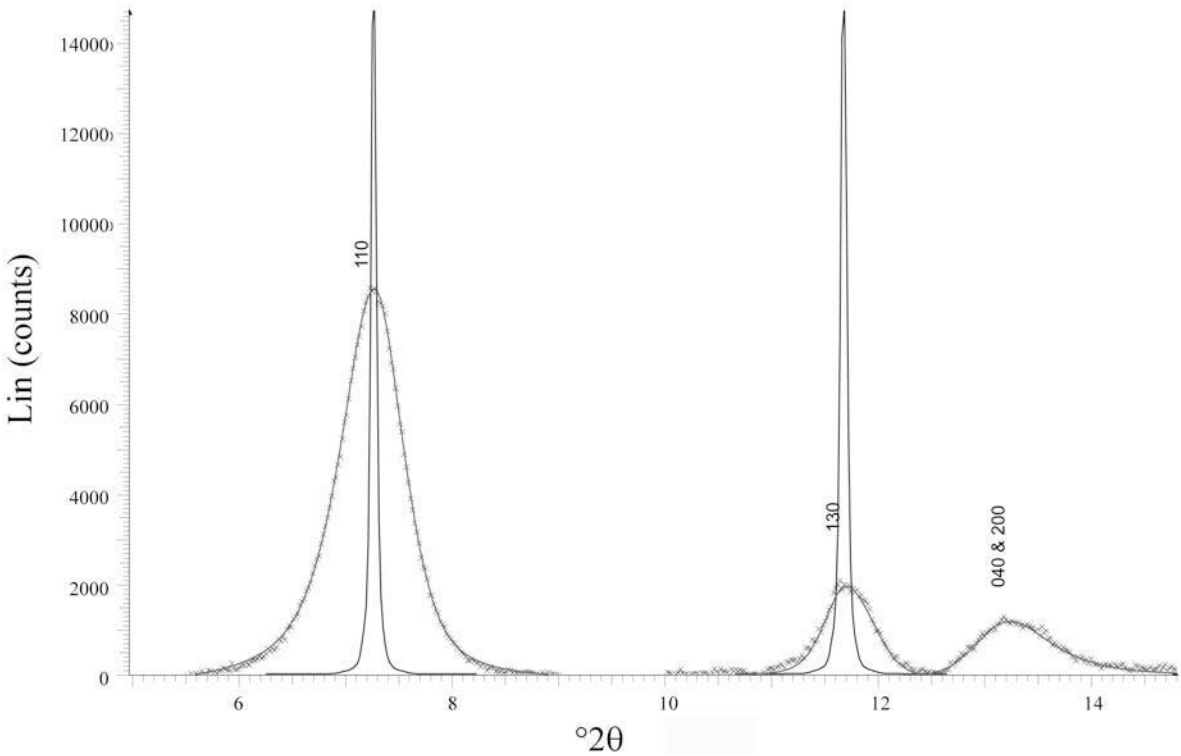


Figure 3. Close-up of the 5–16°2θ section of the fitted profiles.

https://doi.org/10.1346/CCMN.2006.0540310 Published online by Cambridge University Press

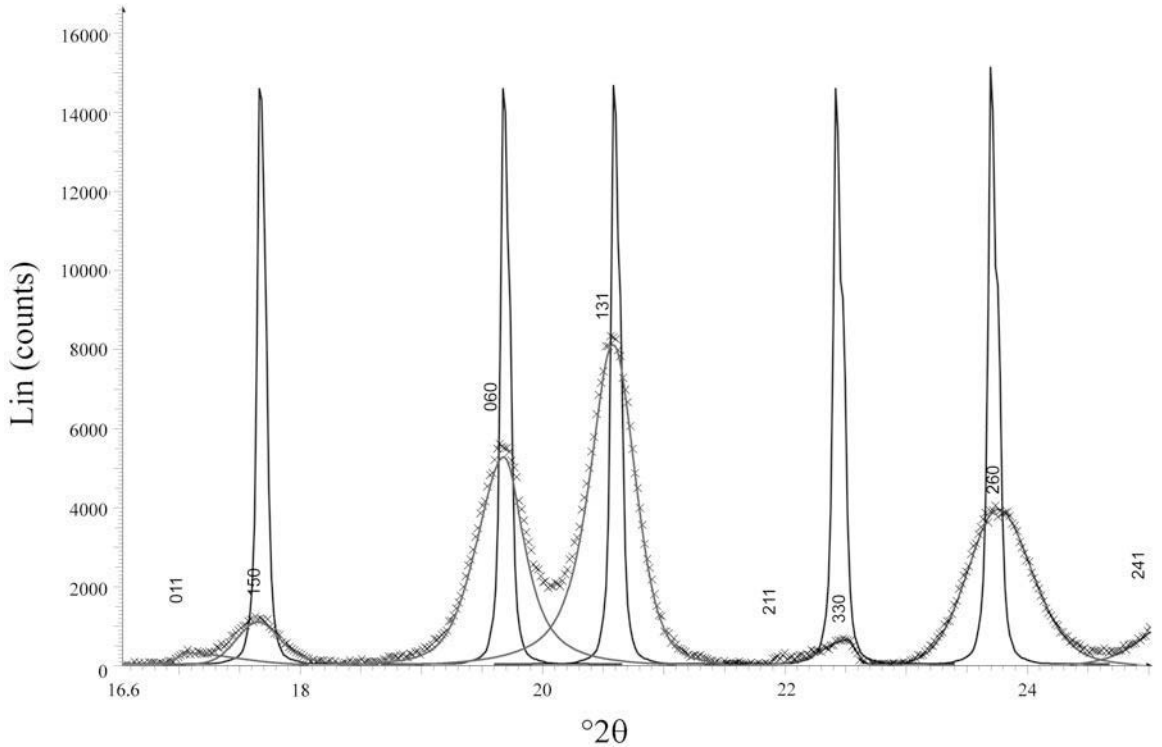


Figure 4. Close-up of the 16–25º2θ section of the fitted profiles. The fitted profile of 211 is not included to avoid cluttering the diagram.

are are presented, after background subtraction, in Figure 2 (lower) (note the different counting time, 4 s for the 110 peak and 16 s for the other peaks), the corresponding standard profiles used for microstructural XRD analysis are also shown (narrow profiles).

Figure 2 shows that there is no significant overlap for the selected peaks (110, 130, 150, 060, 330 and 260); this enables the fitting of each profile. Instead of line overlapping (011 and 150, 060 and 131, 211 and 330) the Profile program allowed us to extract the individual components of each diffraction line. Experimental and fitted profiles for XRD microstructural anlysis of a sample with 3 s grinding, as well as the corresponding standard profiles are shown in Figures 3 and 4. Peaks *h*00 were not selected on the basis of the micromorphological approach (note, moreover, the strong overlap of the 200 and 400 reflections), because the (100) face with small central distances does not appear, and so no comparison with micromorphological observations could be made if XRD microstructural data were obtained.

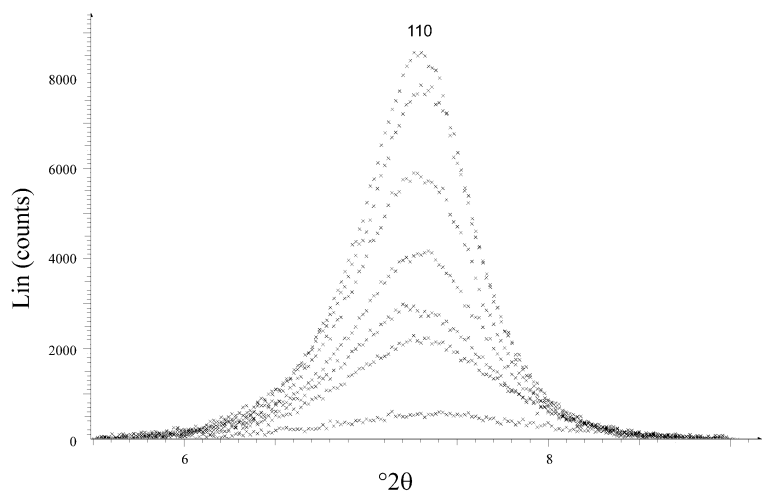


Figure 5. Peak 110 in the different samples (from N3, uppermost, to N60, lowermost).

https://doi.org/10.1346/CCMN.2006.0540310 Published online by Cambridge University Press

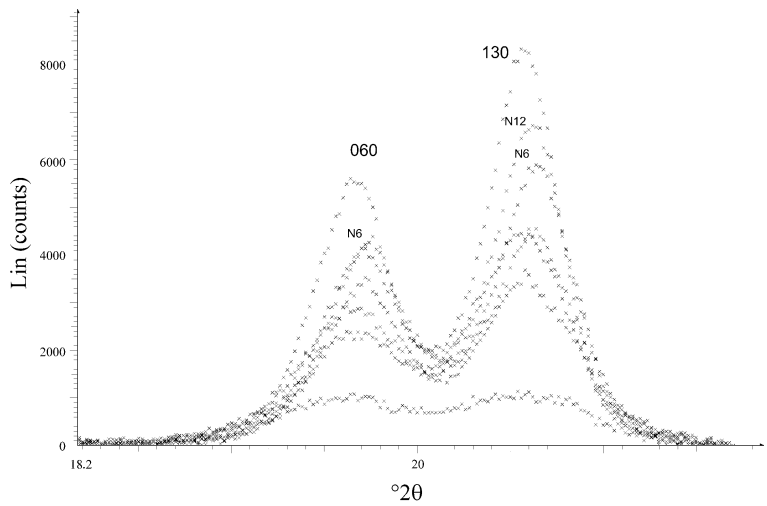


Figure 6. Peaks 060 and 131 for different samples (from N3, uppermost, to N60, lowermost; the second highest peak for reflection 131 corresponds to N12, but not for 060).

Moreover, all these *h*00 peaks are severely overlapped by different peaks at the same position, *e.g.* 200 and 040.

The 0*k*0 peaks are severely overlapped, except for 060. For the 060 and 131 profiles, good fits were achieved (see the range 18.5–21.5º2θ in Figure 4), as shown for these profiles of sample N3 by the R_{wp} values in Table 2. The 020 peak (neighbor of 110, present in the calculated pattern 75-1597, and not present in the 26-1226 file) was not distinguished. The neighboring peaks to the 0*k*0 peaks are labeled in Figure 2, and there are no other 0*k*0 peaks at higher angles.

The 110 and 330 reflections, as well as those at 130 and 260, are not significantly overlapped by neighboring peaks and so these four reflections can be used in this case for double-line analysis with the Warren-Averbach method. The same profiles and those of 150 and 131 are also studied by the simplified single-line method of the Voigt function. The enlargement in Figure 4 shows in more detail the peaks of lower intensities (150 and 330).

Table 2 shows the parameters of the modeled profiles for the different peaks considered and the values of the microstructural parameters calculated using the Voigt function method. The value of FWHM for each peak increases with grinding time (four anomalies can be observed, in N6 for 130, 330 and 150, and in N36 for 330, and only the two last cases with increases of >5%). The peaks 110, 060 and 131 for the different samples are shown in Figures 5 and 6.

Table 3 shows some microstructural parameters obtained using the Warren-Averbach method. For [130] in N60 and for [110] in N48 and N60, no results were obtained due to disappearance of corresponding peaks. Figure 7 shows the evolution of distributions of cumulative frequencies of crystallite size for both directions studied by this method (only the distributions for the N3 sample and for the greatest grinding time providing results are represented). The displacement of the cumulative curves for [110] is very short and quite clear for [130]. The values of average column length are also shown in graphics of Figure 8 (as open squares).

The evolution of apparent crystallite size obtained using the Voigt function method $\langle D_v \rangle$ (filled circles) is also shown in Figures 8 and 9. The $\langle D_v \rangle$ values are greater than the corresponding values of average column length (L) obtained using the Warren-Averbach method. The values of apparent crystallite sizes for diffraction directions 130 and 150 are in geometric disagreement (they should be smaller in a crystallite of form {010} or {110}, for 130 direction of diffraction).

The correlation of L and $\langle D_v \rangle$ values in the 130 direction is quite good for 260 and worse for 130. Considering that a contribution of strain to line broadening has been found for two directions, using the

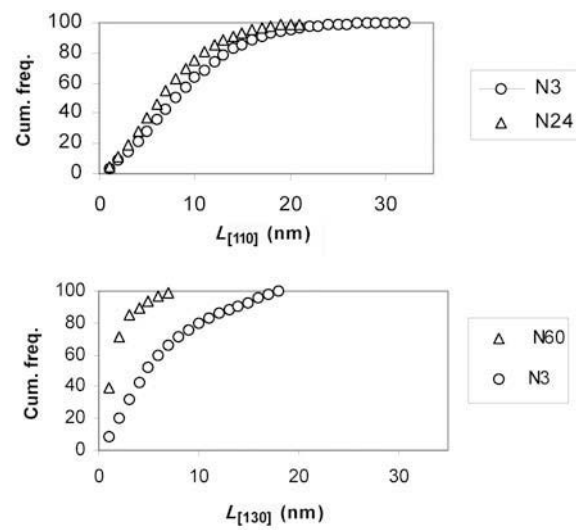


Figure 7. Evolution of the crystallite-size distribution obtained by the Warren-Averbach method for the 110 and 130 directions of diffraction.

https://doi.org/10.1346/CCMN.2006.0540310 Published online by Cambridge University Press

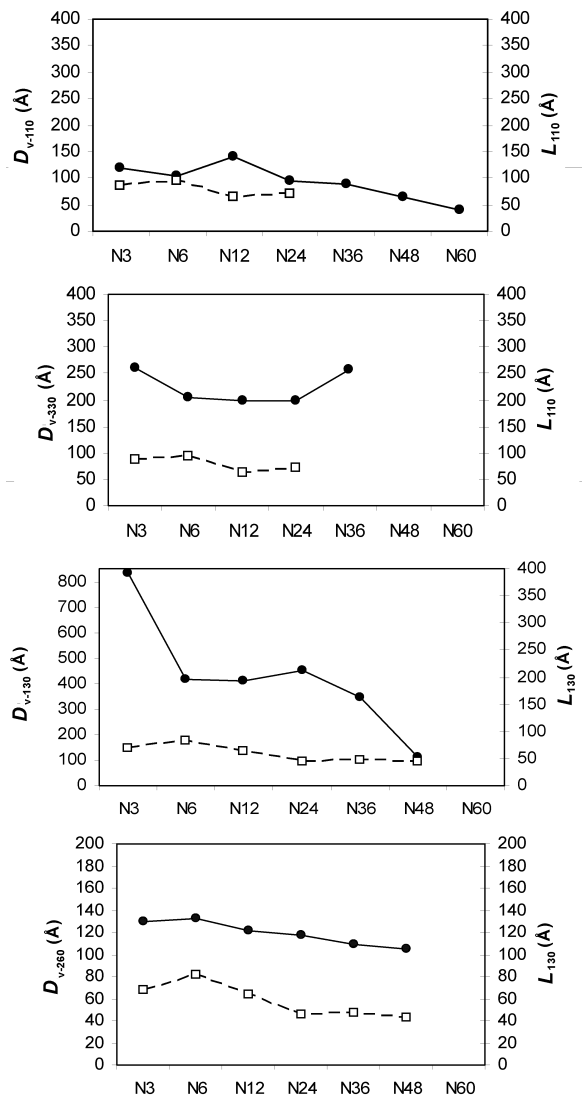


Figure 8. Evolution of crystallite sizes (Å) from the 110, 330, 130 and 260 peaks for the different samples. Squares, for average column length (L) by the Warren-Averbach method. Circles, for average crystallite size, by the Voigt function method.

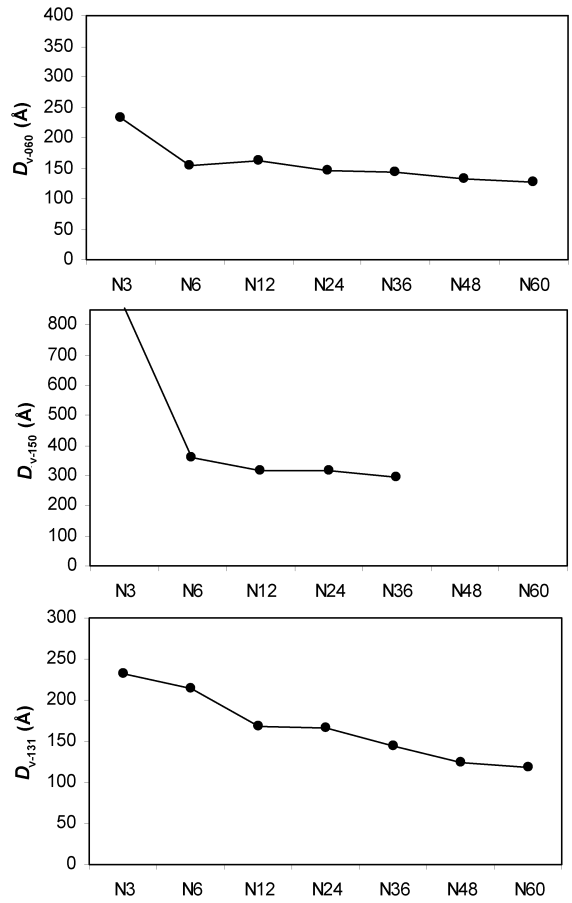


Figure 9. Evolution of crystallite sizes (Å) from the 060, 150 and 131 peaks for the different samples. Average crystallite size by the Voigt function method.

Warren-Averbach method, it is reasonable to assume that there is a strain contribution to the broadening in other directions. Even though the Voigt function method provides useful values to compare the microstructural evolution with grinding time for all the considered directions, it must be noted that the method involves the significant assumptions of size and strain profiles as Lorentzian and Gaussian, respectively (Langford, 1978, 1992).

The changes of the apparent crystallite size corresponding to faces of greater morphological expression (110 and 010) with the grinding time are noticeable but not rapid.

Figures 8 and 9 allow us to compare the general trends of more or less noticeable decrease of crystallite size $<D_v>$. The decrease is observed mainly for grinding times changing from 3 to 6 s, and is very evident for reflections 060, 150 and 130. The differences for $hk0$ diffraction directions must be related to failures along the water channels which are parallel to 001, (010) and (100) according to the structure model of Brauner and Preisinger (1956); for $1k0$ planes in particular, the higher k is, the more channels are cut. Smaller final decreases of $<D_v>$ for 060 can be understood in the same way (minimum of available failure directions is related to the channels of water in the normal direction).

It follows from the comments about Table 1 and Figure 1 above, that the elongated faces recognized in FESEM images of N3 (Figure 10,a,b,c,f) must correspond to the {010} and {110} forms. These images show clearly that the mechanical comminution causes a decrease of the modal aspect ratio (length/width value) of rectangular faces (prevalent in particles).

Figure 10a,b shows the changes in the sample with increasing grinding time. Sample N3 consists of bundles of sepiolite laths which are more or less isolated, while N36 shows shorter laths with agglomerates of finer particles originating from the broken laths with some

https://doi.org/10.1346/CCMN.2006.0540310 Published online by Cambridge University Press

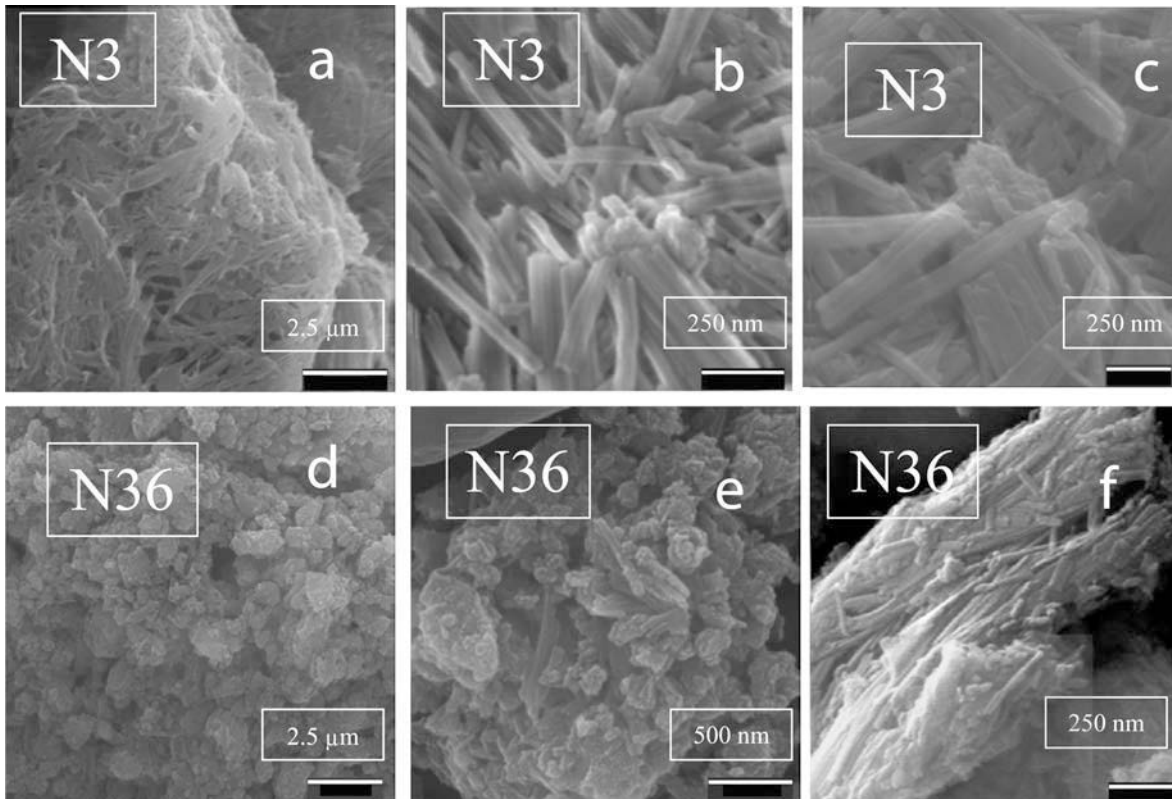


Figure 10. FESEM images of samples N3 (a,b,c) and N36 (d,e,f). Micrographs a and d show N3 and N36 at low magnification. The shortening and thinning of sepiolite laths can be observed in f (compared to c). The agglomeration of finer particles resulting from grinding is shown in e (compared to b, where isolated laths are prevalent). Micrograph f shows welded shortened laths in sample N36.

remaining longer. The lengths of laths are clearly shortened with increased grinding time, from >2000 nm (N3) to mostly <500 nm (N36).

Measurements of widths in rectangular faces (317 cases) on FESEM images of N3 sample.

Two ranges of values include >90% of measured values: (12−25 nm) 51.5% and (25−40 nm) 41.4%. The values found in the whole sample for mode, average and standard deviation were 19.65, 26.8 and 8.69 nm, respectively. Both ranges of measurements must correspond to the most probable faces: that of {110} prisms and {010} pinacoids and both ranges are included in the range of thickness (15−100 nm) measured using transmission electron microscopy in {110} prisms of another sepiolite by Martin Vivaldi and Robertson (1971).

The lengths of these laths in sample N3, measured using FESEM, are much greater than the domain sizes (say 10−100 nm) producing diffraction broadening (Klug and Alexander, 1972); the laths must include a lot of crystallites queued along axis [001], and the decrease of FESEM length for N36 must be related to a decrease in that number.

In addition to that decrease in the number of crystallites of the laths along [001], there is also a decrease of the average crystallite size contributing to the diminution of surface area observed for up to 36 s of grinding (see the surface area measured by the BET method for the different samples on Table 4), and that is in agreement with the microstructural evolution found by Kojdecki *et al.* (2005).

The observed values of surface area (Table 4) are in the range of the experimental values found by Hibino *et al.* (1995) for different sepiolite specimens (except for a small value for the sample ground for 60 s). The decrease in the surface area with an excessive increase in grinding time was also observed by Cornejo and Hermosin (1988) in ball milling and was interpreted by

Table 4. Surface area (m^2/g) of the studied samples by the BET method.

Sample	N3	N6	N12	N24	N36	N48	N60
	172	215	225	220	286	233	120

https://doi.org/10.1346/CCMN.2006.0540310 Published online by Cambridge University Press

the authors to be the result of the coverage of the particle surface by a protective amorphous coating.

CONCLUSIONS

Powder XRD analysis has been used to show some features of the evolution of sepiolite in vibrating dry milling. A continuous increase in FWHM values has been observed for the 110, 131 and 330 peaks with milling time from 3 to 24 s; small anomalies have been found from 3 to 12 s for peaks at 130, 150, 260, and at 36 s for the 330 peak. The existence of a strain contribution to line broadening has been proven by the Warren-Averbach method. The general trends of decreasing apparent crystallite size (with possible anomalies) and of increasing strain parameter (also with possible anomalies) up to a top value (for a short milling time, when compared to equivalent times in ball milling) have been observed by means of the XRD and the simplified method of the Voigt function.

The observed differences in decreases of crystallite size for the studied directions are related mainly to the orientation of the studied planes with respect to the water channels in the structure of sepiolite, which act as failure directions.

The lengths of rectangular faces (corresponding to the most relevant forms ({110} and {010}) are clearly shortened with the grinding performed, from >2000 nm (at 3 s) to mostly <500 nm (at 36 s). The mechanical comminution procedure clearly causes a decrease in the particle size as well as in the aspect ratio. The BET surface area values, found in the reference sample, are in the range of previously published experimental data for other sepiolites.

The sepiolite aggregates consist of aggregates of lath-shaped agglutinations of crystals with prismatic and pinacoidal faces elongated in the [001] direction (each of them containing several crystallites). A decrease in the number of crystallites along [001] is in agreement with the FESEM observations; the decrease in crystallite size shown by XRD in different directions can correlate with the observed increases of surface area with grinding time. The observed decrease in surface area with grinding time exceeding 36 s must be interpreted as resulting from coating of particles (*i.e.* crystallites) by X-ray amorphous phases.

The anomalies indicated above, relying on a significant increase in crystallite size (two cases for $<D_v>$ and another one for L) and not producing a decrease in surface area must be considered as artefacts appearing during peak handling or introduced by calculations.

ACKNOWLEDGMENTS

The work was carried out during the stay of Marek A. Kojdecki at the University of Valencia (Spain) with financial support from the Spanish Ministry of Education, Culture and Sport (under contract DGU No SB2001-0088), which is gratefully acknowledged.

REFERENCES

Alvarez, A. (1984) Sepiolite: properties and uses. Pp. 253–289 in: *Palygorskite-Sepiolite. Occurrences, Genesis and Uses* (A. Singer and E. Galán, editors). Developments in Sedimentology, **37**, Elsevier, Amsterdam.

Bailey, S.W. (1980) Structures of layer silicates. Pp.1–125 in: *Crystal Structures of Clay Minerals and their X-ray Identification* (G.W. Brindley and G. Brown, editors). Monograph **5**. Mineralogical Society, London.

Bertaut, E.F. (1950) Raies de Debye-Scherrer et répartition des dimensions des domaines de Bragg dans les poudres polycristallines. *Acta Crystallographica*, **3**, 14–19.

Borg, I.Y. and Smith, D.K. (1969) Calculated X-ray powder patterns for silicate minerals. *Geological Society of America Memoires*, **122**, 582–584.

Brauner, K. and Preisinger, A. (1956) Struktur und Entstehung des sepioliths. *Tschechoslowakische Mineralogische und Petrographische Mitteilungen* **6**, 120–140.

Brunauer, P., Emmett, H. and Teller, E. (1938) Adsorption of Gases in Multimolecular Layers. *Journal of the American Chemical Society*, **60**, 309–319.

Caillère, S., Hénin, S. and Rautureau, M. (1982) *Minéralogie des Argiles*, vol. **2**. Mason, Paris.

Causin, P., Nusinovici, J. and Beard, D.W (1989) Specific data handling and new enhancements in a Search/Match program. Pp. 531–538 in: *Advances in X-ray Analysis*, Vol. **32** (C.S. Barret, J.V. Gilfrich, R. Jenkins, T.C. Huang and P.K. Predecy, editors). Plenum Publishing Corporation, New York.

Clausell, J.V. (2001) Análisis microestructural de caolinita y génesis de caolines en el Macizo Ibérico. *Cadernos Laboratorio Xeoloxico Laxe*, **26**, 11–99.

Cornejo, J. and Hermosin, M.C. (1988) Structural alteration of sepiolite by dry grinding. *Clay Minerals*, **23**, 391–398.

de Keijser, T.H., Langford, J.I., Mittemeijer, E.J. and Vogels, A.B.P. (1982) Use of the Voigt function in a single-line method for the analysis of X-ray diffraction line broadening. *Journal of Applied Crystallography*, **15**, 308–314.

de Keijser, T.H., Mittemeijer, E.J. and Rozendaal, H.C.F. (1983) The determination of crystallite-size and lattice-strain parameters in conjunction with the profile-refinement method for the determination of crystal structures. *Journal of Applied Crystallography*, **16**, 309–316.

Delhez, R., de Keijser, T.H. and Mittemeijer, E.J. (1982) Determination of crystallite size and lattice distortions through X-ray diffraction line profile analysis. Recipes, methods and comments. *Fresenius Journal of Analytical Chemistry*, **312**, 1–16.

Donnay, J.D.H and Harker, D. (1937) A new law of crystal morphology extending the law of Bravais. *American Mineralogist*, **22**, 446–467.

Dowty, E. (1980) Computing and drawing crystal shapes. *American Mineralogist*, **65**, 465–471.

Grim R.E (1968) *Clay Mineralogy*. Mc Graw-Hill, New York, 596 pp.

Guinebretière, R. (2002) *Diffraction des rayons X sur echantillons polycristallins*. Hermes Science Publications, Paris, 287 pp.

Harben, P. and Kuzvart, M. (1999) *Industrial Minerals: A Global Geology*. Industrial Minerals Information plc, London, 476 pp.

Hibino, T., Tsunashima, A., Yamazaki, A. and Otsuka, R. (1995) Model calculation of sepiolite surface areas. *Clays and Clay Minerals*, **43**, 391–396.

ICDD (2002) *PDF-2 on CD-ROM, Release 2002*. International Centre for Diffraction Data. Pennsylvania.

Jones, B.F. and Galán, E. (1988) Sepiolite and palygorskite. Pp. 631–674 in: *Hydrous Phyllosilicates* (S.W. Bailey,

https://doi.org/10.1346/CCMN.2006.0540310 Published online by Cambridge University Press

editor). Reviews in Mineralogy, Vol. **19**. Mineralogical Society of America, Washington, D.C.

Klug, H.P. and Alexander, L.E. (1974) *X-ray Diffraction Procedures for Polycrystalline and Amorphous Materials.* John Wiley & Sons, New York, 965 pp.

Kojdecki, M.A. (2001) Deconvolution by example – computational test of effective algorithms. *Materials Science Forum*, **378–381**, 12–17.

Kojdecki, M.A., Bastida, J., Pardo, P. and Amorós, P. (2005) Crystalline microstructure of sepiolite influenced by grinding. *Journal of Applied Crystallography*, **38**, 888–899.

Langford, J.I. (1978) A rapid method for analysing the breadths of diffraction and spectral lines using the Voigt function. *Journal of Applied Crystallograpy*, **11**, 10–14.

Langford, J.I. (1992) The use of the Voigt function in determining microstructural properties from diffraction data by means of pattern decomposition. Pp. 110–126 in: *Accuracy in Powder Diffraction II* (E. Prince and J.K. Stalick, editors). Special Publication, National Institute of Standards and Technology, Boulder, Colorado, 846 pp.

Langford, J.I and Louër, D. (1996) Powder Diffraction. *Reports on Progress in Physics*, **59**, 131–234.

Lopez Galindo, A. and Sanchez Navas, A. (1989) Criterios morfológicos, cristalográficos y geoquímicos de diferenciación entre sepiolitas de origen hidrotermal y sedimentario. *Boletín Sociedad Española de Mineralogía*, **12**, 399–409.

Martin Vivaldi, J.L. and Robertson, R.H.S. (1971) Palygorskite and sepiolite (the hormites). Pp. 255–275 in: *Electron-Optical Investigation of Clays* (J.A. Gard, editor). Monograph **3**. Mineralogical Society, London.

Mittemeijer, E.J. and Scardi, P., editors (2003) *Diffraction Analysis of the Microstructure of Materials*. Springer-Verlag, Berlin, 552 pp.

Nagata, H., Shimoda, S. and Sudo, T. (1974) On dehydration of bound water sepiolite. *Clays and Clay Minerals*, **22**, 285–293.

Niskanen, E. (1964) Reduction of orientation effects in the quantitative X-ray diffraction analyses of kaolin minerals. *American Mineralogist*, **49**, 705–714.

Post, J.L. (1978) Sepiolite deposits of the Las Vegas, Nevada area. *Clays and Clay Minerals*, **26**, 58–64.

Post, J.L. and Janke, N.C. (1984) Ballarat sepiolite, Inyo County, California. Pp. 159–169 in: *Palygorskite-Sepiolite. Occurrences, Genesis and Uses* (A. Singer and E. Galán, editors). Developments in Sedimentology, **37**, Elsevier, Amsterdam.

Rautureau, M. (1974) Analyse structurelle de la sepiolite par microdiffraction electronique. Thèse. Université d'Orleans, France, 89 pp.

Rautureau, M. and Tchoubar, C. (1974) Precisions concernant l'analyse structurelle de la sepiolite par microdiffraction electronique. *Comptes Rendues Hebdomadaires Académie des Sciences de Paris*, **278B**, 25–28.

Rautureau, M. and Tchoubar, C. (1976) Structural analysis of sepiolite by selected area electron diffraction; relations with chemical properties. *Clays and Clay Minerals*, **24**, 43–49.

Santarén, J. and Alvarez, A. (1994) Assessment of the health effects of mineral dusts. The sepiolite case. *Industrial Minerals*, April, 1994, 101–114.

Serrano, F.J., Bastida, J., Amigó, J.M. and Sanz, A. (1996) XRD line broadening studies on mullite. *Crystal Research and Technology*, **31**, 1085–1093.

Serratosa, J.M. (1979) Surface properties of fibrous clay minerals. *Proceedings of the International Clay Conference 1978, Oxford*. Developments in Sedimentology, **27**, Elsevier, Amsterdam, pp. 99–109.

Snyder, R.L., Fiala, J. and Bunge H.J., editors (1999) *Defect and Microstructure Analysis by Diffraction*. IUC Monographs on Crystallography, No. **10**. Oxford Science Publications, Oxford, UK, 785 pp.

Stanton, M.F., Layard, M., Tegeris, A., Miller, E. and Smith, A. (1981) Relations of particle dimension to carcinigenity of amphibole asbestos and other fibrous minerals. *Journal of the National Cancer Institution*, **67**, 965–975.

Vermeulen, A.C and Delhez, R. (2004) Line Profile Analysis (LPA) Methods: Systematic ranking of the quality of their basic assumptions. *Materials Science Forum*. **443–444**, 127–130.

Vicente, M.A., López Gonzalez, J. and Bañares, M.A. (1994) Acid activation of a Spanish sepiolite. Physicochemical characterization, free silica content and surface area of obtained products. *Clay Minerals*, **29**, 361–367.

Virta, R.L. (2004) Clay and Shale. 38 pp. in: *Minerals Yearbook 2003*. URL: http://minerals.usgs.gov/minerals/pubs/commodity/clays/claysmyb03.pdf

Warren, B.E. and Averbach, B.L. (1950) The effect of cold work distortion on X-ray patterns. *Journal of Applied Physiscs*, **21**, 959–999.

Warren, B.E. (1955) A generalised treatment of cold work in powder patterns. *Acta Crystallographica*, **8**, 483–486.

Warshaw, C. and Roy, R. (1961) Classification and scheme for the identification of layer silicates. *Geological Society of America Bulletin*, **72**, 1455–1492.

Wilson, A.J.C. (1967) *Elements of X-ray Crystallography.* Addison Wesley, Reading, Massachusetts, 255 pp.

Wilson, I. (2004) Special clays. *Industrial Minerals*, November 2004, 54–61.

Yücel, A., Rautureau, M., Tchoubar, D. and Tchoubar, C. (1980) Calculation of the X-ray powder reflection profiles of very small needle-like crystals. I. Method. *Journal of Applied Crystallography*, **13**, 370–374.

Yücel, A., Rautureau, M., Tchoubar, D. and Tchoubar, C. (1981) Calculation of the X-ray powder reflection profiles of very small needle-like crystals. II. Quantitative results on Eskiseihir fibres. *Journal of Applied Crystallography*, **14**, 451–454.

(*Received 24 December 2003; revised 23 January 2006; Ms. 870; A.E. Bruno Lanson*)

https://doi.org/10.1346/CCMN.2006.0540310 Published online by Cambridge University Press